IEEE Access
Multidisciplinary ⋮ Rapid Review ⋮ Open Access Journal

Received 3 January 2024, accepted 26 January 2024, date of publication 8 February 2024, date of current version 15 February 2024.

Digital Object Identifier 10.1109/ACCESS.2024.3364073

RESEARCH ARTICLE

Research on the Axial Stability of Large-Capacity Magnetic Levitation Flywheel Driven by Axial-Flux Permanent Magnet Machine Based on Runge-Kutta Method

MINGXIN SUN AND YANLIANG XU
School of Electrical Engineering, Shandong University, Jinan 250061, China
Corresponding author: Yanliang Xu (xuyanliang@sdu.edu.cn)

This work was supported in part by the National Science Foundation of China under Grant U22A2021, and in part by the Science and Technology Major Project of Shandong Province under Grant 2022CXGC020404.

ABSTRACT For high-capacity flywheel energy storage system (FESS) applied in the field of wind power frequency regulation, high-power, well-performance machine and magnetic bearings are developed. However, due to the existence of axial magnetic force in this machine structure along with the uncontrollability of the magnetic bearing, the axial stability of the flywheel needs to be focused on. Firstly, a FESS with an axial flux permanent magnet synchronous machine (AFPMSM) based on soft magnetic composite (SMC) material and HALBACH axial passive magnetic bearing (PMB) structure is proposed, and its principle and structural superiority are introduced. Secondly, a three-dimensional (3D) finite element method (FEM) simulation model of the machine and bearing is established. The effects of current, air gap and bearing parameters on the rotor axial force are investigated using the 3D FEM. In addition, the relationship between current and displacement on axial force is fitted by the response surface method (RSM). The startup process and the effect of current change on displacement of the flywheel under different operating conditions are investigated by the Runge-kutta (RK) method. After that, the rotor displacement under various air gaps and bearing forces is studied to ensure that the rotor displacement is smaller than the air gap, thereby ensuring the flywheel rotor stays within a controllable range. Finally, the FESS prototype is manufactured and tested, which finally enables it to operate safely and stably.

INDEX TERMS Flywheel energy storage system (FESS), axial-flux permanent magnet synchronous machine (AFPMSM), axial magnetic bearing (AMB), Runge-Kutta (RK) method, response surface modeling (RSM), axial stability.

I. INTRODUCTION

Among the various forms of energy storage currently applied on a large scale, flywheel energy storage system (FESS) has the characteristic of being able to realize high-power rapid charging/discharging (C&D), and it is widely used in the fields of grid peaking and frequency regulation, electric vehicle, aerospace, and uninterruptible power supply (UPS), etc [1], [2], and [3]. FESS mainly consists of flywheel rotor, motor/generator, bearing, vacuum chamber, power converter and controller [4], of which the motor/generator is the key component to realize the electromechanical energy conversion of FESS, thus an efficient and reliable machine plays an important role for FESS [5]. At present, FESS machine mainly include asynchronous machine, reluctance machine, induction machine, permanent magnet synchronous machine (PMSM), etc. [6], [7], and [8], of which PMSM have great development prospects due to their advantages of simple structure, high operating efficiency and high power density, etc. [9]. The traditional radial flux PMSM has a

The associate editor coordinating the review of this manuscript and approving it for publication was Feifei Bu.

long winding end, which occupies a large amount of axial height. And its cogging torque is large, which makes the machine fabrication and assembly difficult and unfavorable for bearing support [10]. Axial-field permanent magnet synchronous machine (AFPMSM), are characterized by short axial size, light weight and compact structure, high efficiency, and high power density [11], which is more suitable for large-capacity FESS [12], [13]. However, it is difficult to apply the structure of a two-rotor disk machine to FESS because the flywheel rotor is placed in parallel with the disk machine [14]. The single rotor single stator structure is the simplest structure among the AFPMSM and is the basis for other forms of derivation [15]. But the disadvantage of this structure is that the axial magnetic force between the stator and rotor is large, thus the requirement for the axial bearing performance of the machine during operation is high [16].

For large-capacity FESS, low loss and large-capacity bearing which can withstand high rotational speed is the critical for research [17]. As a kind of non-contact bearing with wide application, magnetic bearing can be further divided into permanent magnetic bearing, active magnetic bearing, and superconducting magnetic bearing [18]. Among them, PM bearing utilize the suction or repulsion support between PMs, which have the advantages of small size, no power consumption, and simple structure [19]. Especially, the PM passive magnetic bearing (PMB) can play the role of large-size flywheel rotor weight unloading by utilizing the axial force between the PMs [20]. However, due to the uncontrollability of the PMB, the axial magnetic force of the AFPMSM will have a certain impact on the load carrying stability of the axial PMB, and the axial vibration that may occur during the operation of the flywheel needs to be focused on [21]. While for radial magnetic bearing (RMB), active control is usually used, with better stability in the radial direction.

The displacement of the flywheel rotor is mainly due to its force imbalance, so modeling this differential equation of motion of the flywheel rotor based on a AFPMSM and axial PMB is the key to solving the axial displacement of the rotor. Response surface modeling (RSM) is one of the commonly used approximate agent models that characterize the relationship between output variables and input variables by constructing a response surface approximate algebraic model [22]. In addition, in numerical analysis, the Runge-kutta (RK) method is a single-step algorithm, which includes Euler method, improved Euler method, for solving the numerical solution of ordinary differential equations [23]. This algorithm is widely used in engineering due to its high accuracy. The more commonly used of the various Runger-Kutta methods is the fourth order Runge-kutta (RK4) method [24]. This method is mainly in the known derivatives of the equation and the initial value of information, applied in computer simulation, eliminating the complex process of solving differential equations. In this paper, the finite element method, response surface method and RK4 are utilized to study the axial displacement of the flywheel under different operating conditions, and then the influence of the design parameters of the motor and bearings on the axial displacement is deduced to ensure the stability of the operation of this flywheel system.

The main innovations of this paper are as follows:

First, an AFPMSM based on SMC material and HALBACH axial PMB structure are proposed in this paper for a high-capacity, high-power FESS in the field of wind power frequency regulation. The machine and bearing make the flywheel system more compact, the axial height of the flywheel is compressed, and the internal space of the flywheel is reasonably utilized, which is conducive to bearing support. In addition, the bearing loss is low, which improves the efficiency of the FESS. Compared with other types of FESS with the same power and capacity, this structure has a lower axial height and higher efficiency.

Secondly, it focuses on the axial vibration problems that may be brought by this machine and bearing structure, and the axial displacement caused by the unilateral magnetic force of the AFPMSM is seldom researched at present. Considering the effects of bearings, machine parameters and current disturbance on the axial force of the machine and bearing, the axial displacements of the flywheel rotor under different operating conditions are investigated by using the RK4 and RSM.

Finally, by studying the rotor axial displacement when changing the machine air gap and bearing axial force, the relationship between the design parameters of the machine as well as the bearing and the axial displacement is obtained in this paper, which ensures the stability of the operation of this FESS, and it is of great significance for the optimization and design of future eFESS based on the AFPMSM and the HALBACH axial PMB.

Based on the series of issues presented above, this paper is organized as follow:

The section II introduces the structure of FESS. The finite element method (FEM) is used to analyze the characteristics of the axial force of the flywheel under different working conditions, and to study the influence of the current, displacement and bearing structure parameters on the axial force of the flywheel in the second section.

In the section III, the equations of the relationship between current and displacement and axial force are fitted by the RSM, and then the RK method is used to study the starting process and the effect of sudden change of current on the displacement.

In the section IV, the rotor displacement under different air gap and different bearing force is investigated to obtain the relationship between the air gap, bearing force and the maximum rotor displacement.

The prototype of the 500 kW FESS is developed and the experiments are conducted in the section V. The section VI is the conclusion.

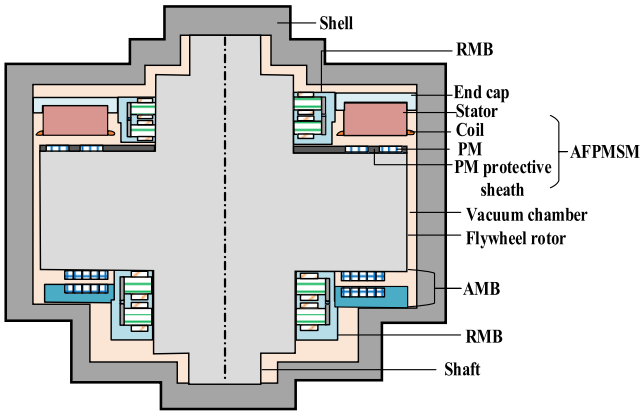

FIGURE 1. The structure of FESS.

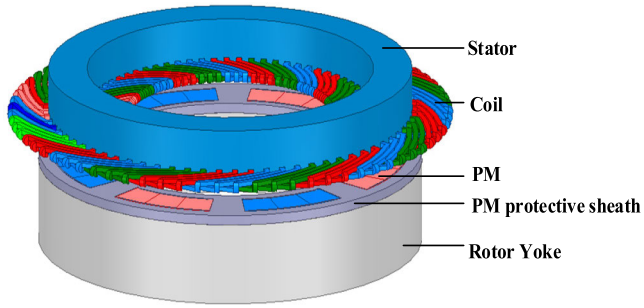

FIGURE 2. The structure of AFPMSM.

II. STRUCTURE OF MAGNETIC LEVITATION FLYWHEEL

The FESS consists of five main components: flywheel rotor, bearing, motor/generator, C&D converter, and vacuum chamber, which is usually installed vertically with its structure shown in Fig. 1. The AFPMSM utilizes the flywheel rotor as the machine rotor yoke, and the machine is placed parallel to the upper side of the flywheel rotor. In addition, the FESS includes two RMB and one axial magnetic bearing (AMB) to achieve stable levitation in three degrees of freedom.

A. AFPMSM

Among them, An AFPMSM based on soft magnetic composite (SMC) for high-capacity FESS is proposed. The AFPMSM adopts an 8-pole/72-slot single stator single rotor structure, as shown in Fig. 2, which mainly consists of stator core, winding, rotor core, permanent magnets (PMs) and PM sheath. The The stator core is made of SMC material, and the windings adopts the form of integer slot distribution winding, which are wound in the stator slots. The axially magnetized SmCo28 PMs, arranged in alternating N and S arrangements, are mounted on the rotor yoke and each pole is protected by a non-conductive sheath. In addition, the eddy current loss of the PMs can be reduced by dividing the PMs along the circumferential direction. The AFPMSM based on SMC can eliminate the high frequency core loss of the stator, thereby increasing machine efficiency, while making the flywheel more compact and effectively compressing the axial height of the flywheel. In addition, the unilateral axial magnetic force generated by the AFPMSM plays a unloading effect on the gravity of the flywheel, which is conducive to reducing the bearing load.

TABLE 1. Radial magnetic bearing structure design parameters.

Parameter	Value	Parameter	Value
Outer diameter of stator core	330mm	Length of PM magnetization direction	20mm
Outer diameter of stator core pole shoe	230mm	Inner diameter of stator core pole shoe	210mm
Inner diameter of PM	310mm	Outer diameter of PM	370mm
Outer diameter of stator teeth	260mm	Outer diameter of rotor core	208mm
Axial length of stator core	60mm	Inner diameter of rotor core	170mm
Stator pole width	120mm	Axial length of rotor core	80mm
Number of control coil turns per pole	150	Wire diameter	0.51mm

B. BEARING

For bearing, firstly a permanent magnet radial magnetic bearing (PMRMB) is proposed, which is composed of stator core, PM, magnetic ring, control winding as shown in Fig. 3(a) and its main dimensional parameters are shown in Table 1. It adopts active control, which can adjust the control current so as to change the air gap magnetic field on both sides of the rotor and ensure the radial stabilization of the rotor levitation.

Ordinary permanent magnet passive magnetic bearings utilize the suction or repulsion between permanent magnets to work without external power control, with a simpler structure and lower loss. And a HALBACH magnet structure, can form a special magnetic field, through the combination of different magnetization direction magnets, not only can get a good sinusoidal air gap density distribution, but also can further improve the air gap density and magnetic flux. Applied to permanent magnet axial passive magnetic bearing (PMB), it can realize higher support strength with the same volume of permanent magnet material compared with traditional PMB.Therefore, a structure of HALBACH axial PMB is proposed as shown in Fig. 3(b), which can realize a higher support strength with the same volume of PM compared to the traditional PMB. The PMB is located under the flywheel rotor, which contains two bearing disks, where the upper is a moving plate and the lower is a static plate, and there is an air gap before both of them in order to realize levitation. The HALBACH axial PMB consists of 9 rings of PMs, with a radial thickness of 17 mm and an axial height of 30 mm each, which are made of SmCo28 material. Between each ring of PMs, there are magnetic spacer rings with a thickness of 1.5 mm. Due to the large inner and outer diameter of the PMs, in which the outer diameter of the PMs ring is 815 mm and the inner diameter is 485 mm, the processing usually needs to be divided into pieces, and the number of pieces is about 30∼40 pieces for each ring.

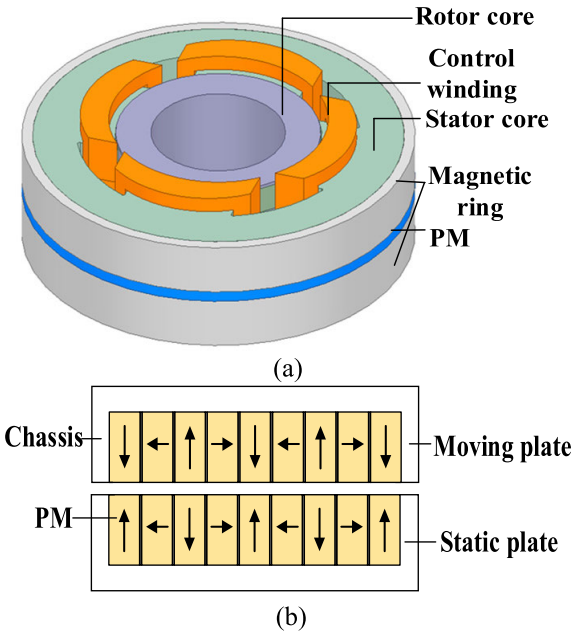

FIGURE 3. The structure of bearing. (a)PMRMB (b) Axial PMB.

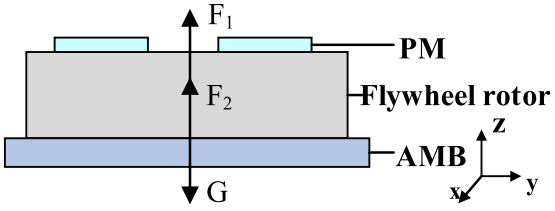

FIGURE 4. Flywheel rotor force.

III. THE CHANGE CHARACTERISTICS OF FESS AXIAL FORCE

The axial force on the flywheel rotor is shown in Fig. 4. Only the axial force is considered, the force on the rotor mainly consists of the electromagnetic force F_1 along positive direction of the Z-axis, the bearing support force F_2, and the gravity G of the flywheel rotor. Due to the large capacity of this flywheel energy storage system, the rotor weight can be up to 10000 kg, so its own gravity G is about 100 kN.

From the FESS force analysis, it can be seen that when the weight of the flywheel rotor is determined, it is necessary to reasonably design the electromagnetic force and bearing capacity. Therefore, it is required to use the FEM to analyze the influence of air gap and bearing parameter variations on the electromagnetic force and bearing capacity of the machine.

In this paper, ANSYS MAXWELL 2020R1 version software is used to establish the three-dimensional finite element simulation model of the motor, whose mesh dissection is a crucial step in the simulation, which affects the accuracy of the calculation results. Because the structure of the axial flux permanent magnet synchronous motor is more complex, thus triangle, quadrilateral and tetrahedron are used for meshing in this paper, and the total number of meshes is 258946.

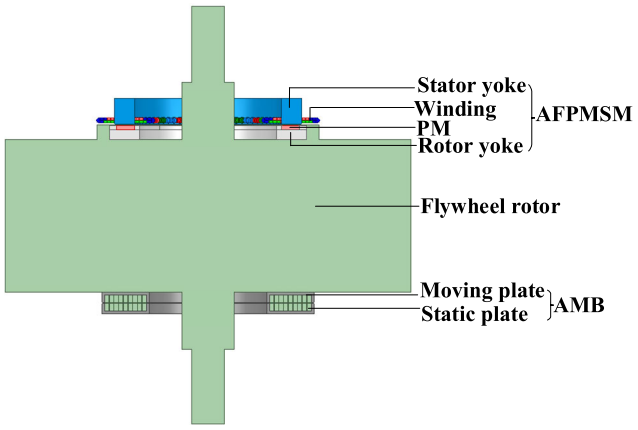

FIGURE 5. FEM model structure.

TABLE 2. Air gap and axial force when the rotor is in force balance.

Condition	Machine air gap/mm	Bearing air gap/mm	F_1/kN	F_2/kN	(F_1+F_2) /kN
No-load	6	5.7	22.6	77.4	100
Generator	6	5.2	22.6	77.4	100
Motor	6	6	22.6	77.4	100

In addition, finite element simulation is essentially an iterative process, and the convergence of the solution needs to be taken into account in the simulation, so the nonlinear error and convergence criterion of the axial flux permanent magnet synchronous motor model in this paper are set to 0.005.

A. THE EFFECT OF DISPLACEMENT ON THE AXIAL FORCE

Since the axial PMB is placed at the bottom of the flywheel rotor, the moving plate of the PMB is connected to the flywheel rotor, utilizing the flywheel rotor instead of the AFPMSM rotor yoke. When the rotor displacement occurs, the corresponding motor air gap and bearing air gap both change. Therefore, when investigating the effect of displacement changes on the electromagnetic force of the motor and bearing capacity, a combined FEM simulation model of a AFPMSM and axial PMB is established, and the model structure is shown in Fig.5.

Firstly, the machine air gap of 6 mm is kept constant to study the air gap size and axial forces when the rotor is in force balance under the three operating conditions as shown in Table 2. Afterwards, when the rotor is displaced, the corresponding machine air gap and bearing air gap are changed, and the magnetic field distribution of the machine and bearing will be different, which results in the change of each axial force on the rotor with displacement as shown in Fig.6.

As can be seen from the figure, when the rotor moves downward, the machine air gap increases and the bearing air gap decreases, resulting in a decrease in the F_1 and an increase in the F_2. But the change of F_2 is bigger than F_1,

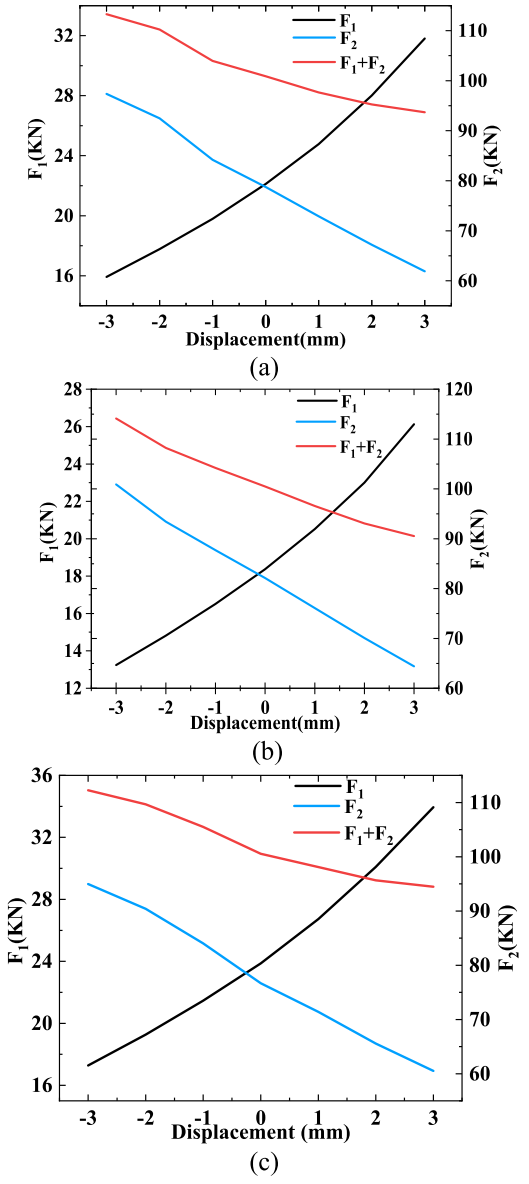

FIGURE 6. Variation of each axial force on the rotor with displacement. (a) No-load (b) Generator. (c) Motor.

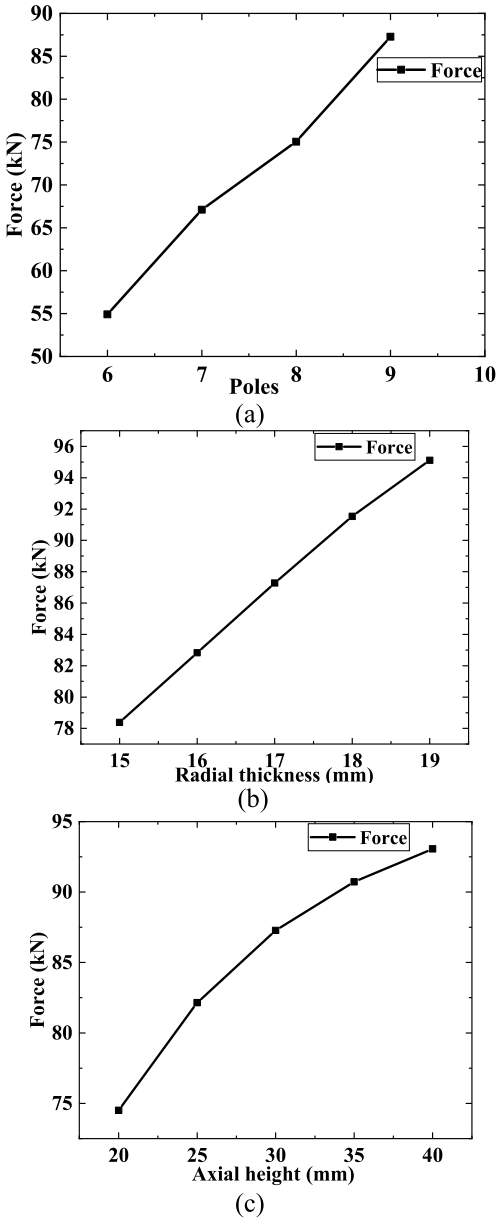

FIGURE 7. Relationship of bearing capacity with PMs parameters. (a) Bearing force-PM poles. (b) Bearing force-PM radial thickness. (c) Bearing force-PM axial height.

so the combined force increases, greater than G. Conversely, when the rotor moves upward in the positive direction along the Z-axis, the combined force decreases and is less than the rotor gravity G. When the rotor is stably suspended, the sum of F_1 and F_2 is equal to the G. Once there is an electromagnetic disturbance in the magnetic field, the rotor is subjected to changes in the electromagnetic force, and the rotor is unbalanced, which will produce a certain amount of axial displacement.

B. THE EFFECT OF STRUCTURE PARAMETERS ON BEARING CAPACITY

According to the structure of PMB, it is known that the bearing capacity is mainly related to the number, radial width, axial height pf PMs and size of air gap, so different bearing capacity can be realized by designing these parameters. The FEM is used to establish a 3D model of HALBACH axial PMB and analyze its axial load capacity. Under the same air gap of 6mm, the bearing capacity is related to the change of number, radial thickness and axial height of PMs as shown in Fig. 7.

C. THE EFFECT OF CURRENT ON THE ELECTROMAGNETIC FORCE

When the rotor is stably suspended, the combined force of F_1 and F_2 is equal to G. Once there is interference in the magnetic field, the electromagnetic force changes, and the rotor force is unbalanced, which will produce axial

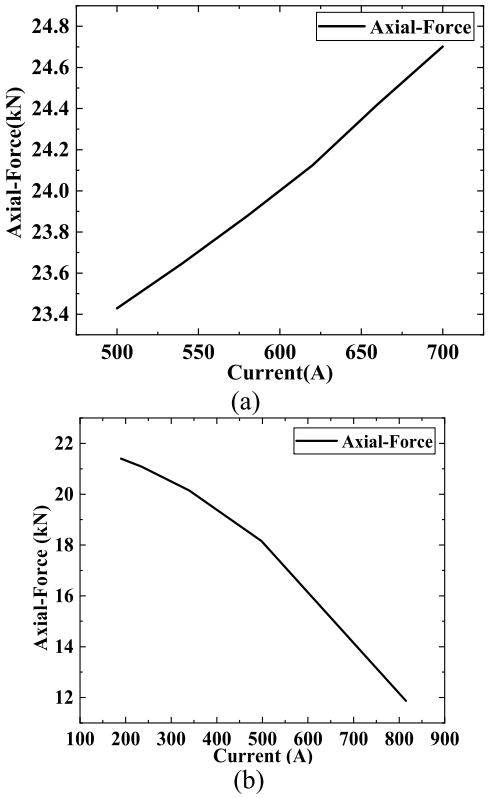

FIGURE 8. Effect of current on machine axial force. (a)Motor. (b)Generator.

displacement. A three-dimensional (3D) FEM model of the AFPMSM based on SMC is established to analyze the effect of current on the axial magnetic force of the machine under different conditions, as shown in Fig.8. Firstly, for the motor, as the input current increases, the magnetic force on the rotor increases. Whereas for generator, as the load increases and the output current decreases, the axial magnetic force increases linearly.

IV. RESEARCH ON AXIAL DISPLACEMENT OF FESS ROTOR

A. THE ESTABLISHMENT OF DIFFERENTIAL EQUATIONS BY RUNGE-KUTTA METHOD

The equations for the electromagnetic force F_1, bearing capacity F_2, displacement x, and current i are obtained by fitting the above relationships using the RSM as in (1)-(3).

$$F_2(x) = 77.36 - 9.759x \tag{1}$$

$$F_1(x,i) = 0.084 + 2.552x - 0.002765i + 0.1903x^2 + 0.003705xi + 7.938\text{E}-06i^2 \tag{2}$$

$$F_1(x,i) = 0.03245 + 2.751x - 0.005374i + 0.1849x^2 - 0.000782xi - 7.568\text{E}-06i^2 \tag{3}$$

Dynamic analysis is carried out using the fourth-order Runge-kutta (RK4) method, and the force balance equations are established as follows in (4) firstly.

$$ma = F_\text{h} - mg = F_1 + F_2 - mg \tag{4}$$

where $a = \ddot{x}$, $v = \dot{x}$, mg = 10000kg。Further the second order differential equation is obtained as follows.

$$\ddot{x} = \frac{F_1 + F_2 - mg}{m} \tag{5}$$

The second order differential equation can be solved using RK4 method by downgrading it so that the initial value is formulated as follows.

$$\begin{cases} y' = f(t,y) \\ y(t_0) = y_0 \end{cases} \tag{6}$$

Then the RK4 of the question can be obtained from the following equation.

$$y_{n+1} = y_n + \frac{h}{6}(k_1 + 2k_2 + 2k_3 + k_4) \tag{7}$$

where

$$\begin{cases} k_1 = f(t_n, y_n) \\ k_2 = f\left(t_n + \frac{h}{2}, y_n + \frac{h}{2}k_1\right) \\ k_3 = f\left(t_n + \frac{h}{2}, y_n + \frac{h}{2}k_2\right) \\ k_4 = f(t_n + h, y_n + hk_3) \end{cases} \tag{8}$$

B. SOLVING FOR ROTOR DISPLACEMENT UNDER MOTOR CONDITION

For different operating conditions, the differential equations and initial values are different, so it needs to be analyzed separately. First of all, for the motor, due to the existence of inductance, the current can not be changed instantaneously, need to analyze the effect of the current change on the rotor displacement in a period of time, to get the differential equation of the motion at this time is as follows.

$$\dot{x} = -0.7207x - 0.0002765i + 0.0903x^2 + 0.0003705xi + 7.938\text{E}-06i^2 \tag{9}$$

$$\begin{cases} \dot{x} = z \\ \dot{z} = \ddot{x} = f(x,i) \\ \dot{y} = C \end{cases} \tag{10}$$

$$\begin{cases} x(1) = 0 \\ z(1) = 0 \\ y(1) = 0 \end{cases} \tag{11}$$

where C is a constant, indicating the slope of the current change in a period of time.

In order to simulate the dynamic change process of current, it can be set as a segmented function as in (12). When considering the starting process of the motor, since the current cannot be changed instantaneously, it is assumed that the starting process can be regarded as the current changing from 0 A to the rated value of 580 A in the course of 20 s and running at the rated current for 10 s, after which the current reaches 600 A via 20 s, and then the current returns to its original rated value after 20 s after running at the current

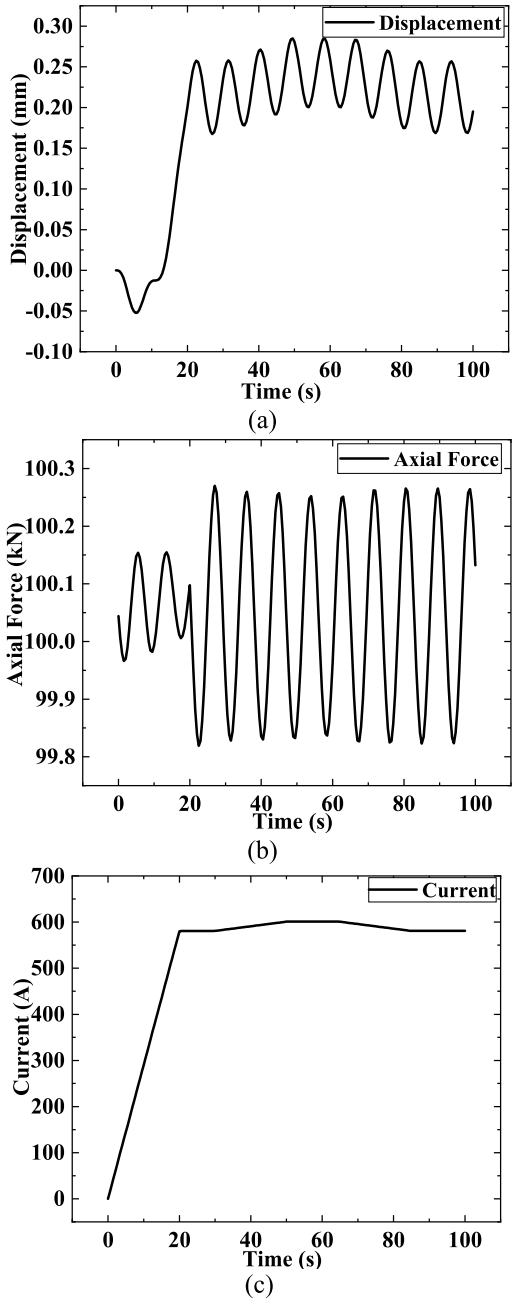

FIGURE 9. Results of motor condition during startup and current change. (a)Rotor axial displacement. (b)Rotor axial force. (c)Current variation.

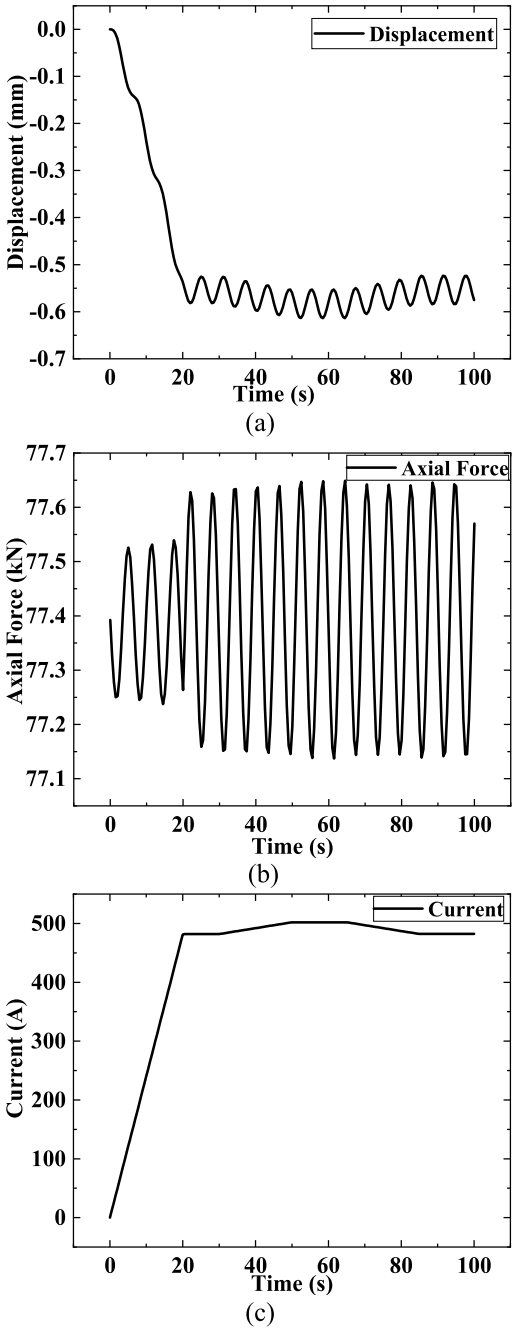

FIGURE 10. Results of generator condition during startup and current change. (a)Rotor axial displacement. (b)Rotor axial force. (c)Current variation.

of 600 A for 15 s, and continues to run at the rated value of 580 A.

$$\begin{cases} \dot{y} = 29\ (t \leq 20\text{s}) \\ \dot{y} = 0\ (20\text{s} < t \leq 30\text{s}) \\ \dot{y} = 1\ (30\text{s} < t \leq 50\text{s}) \\ \dot{y} = 0\ (50\text{s} < t \leq 65\text{s}) \\ \dot{y} = -1\ (65\text{s} < t \leq 85\text{s}) \\ \dot{y} = 0\ (t > 85\text{s}) \end{cases} \tag{12}$$

Using ode45 function to solve the above equations, rotor displacement, rotor force and current variations during the whole process described above is obtained as shown in Fig.9. From the figure, it can be seen that the maximum displacement of the rotor is mainly generated by the starting process, which is about 0.285 mm. The subsequent current disturbance has a smaller effect on the displacement, which is about 0.027 mm.

C. SOLVING FOR ROTOR DISPLACEMENT UNDER GENERATOR CONDITION

For the generator, assuming an external resistive load, the effect of load change on rotor displacement is analyzed for

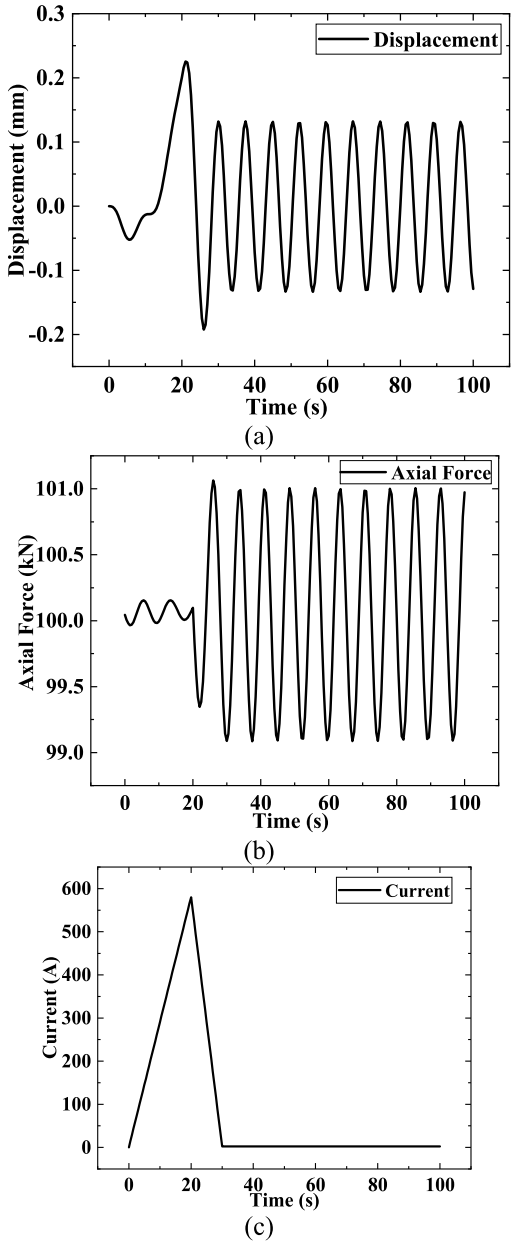

FIGURE 11. Results of no-load condition including the starting process. (a) Rotor displacement. (b) Rotor axial force. (c)Current variation.

a period of time, with the change in current representing the load change. At this time the differential equations are as follows, with the same initial values as for motor.

$$\dot{x} = -0.7008x - 0.005374i + 0.1849x^2 - 0.000782xi - 7.568\text{E} - 06i^2 \quad (13)$$

Similarly the change process of generator load is simulated as in (15). when the startup process is considered, it is assumed that the output current reaches the rated current of 481 A after 20 s. If there is a perturbation in the load, the current increases to 500 A. After 15 s of operation, the current is restored to the rated current, and the operation continues at that current.

$$\begin{cases} \dot{y} = 24.05\ (t \le 20\text{s}) \\ \dot{y} = 0\ (20\text{s} < t \le 30\text{s}) \\ \dot{y} = 1\ (30\text{s} < t \le 50\text{s}) \\ \dot{y} = 0\ (50\text{s} < t \le 65\text{s}) \\ \dot{y} = -1\ (65\text{s} < t \le 85\text{s}) \\ \dot{y} = 0\ (t > 85\text{s}) \end{cases} \quad (14)$$

The curves of rotor displacement, force and current are obtained by solving the above differential equations using RK4 method as shown in Fig.10. From each figure, it can be seen that the generator load and current variations have a greater effect on the rotor displacement than the motor, despite its lower current at rated load. Therefore the maximum rotor displacement is about 0.62 mm and the current perturbation has a lesser effect on the displacement variation, about 0.034 mm, both of which are slightly higher than the motor condition.

D. SOLVING FOR ROTOR DISPLACEMENT UNDER NO-LOAD CONDITION

In addition, when current is 0 A, it is no-load condition and firstly, it is necessary to apply current to make the motor run to the rated speed and then cut off the power. Therefore, the no-load condition can still be solved by using (9)-(11), but the segment function of y needs to be modified as follows in (15). The motor is run at the rated current after 20 s of startup, and since the current cannot be changed instantaneously and suddenly, the current is reduced from 580 A to 0 A after 10 s, and then it is run continuously at no-load.

$$\begin{cases} \dot{y} = 29\ (t \le 20\text{s}) \\ \dot{y} = -58\ (20\text{s} < t \le 30\text{s}) \\ \dot{y} = 0\ (t > 30\text{s}) \end{cases} \quad (15)$$

The curves of rotor displacement and force are obtained by solving the above differential equations using RK4 method as shown in Fig. 11. As can be seen from the figure, the starting process is roughly the same as the motor condition. When the motor is powered off, the rotor oscillates up and down in no-load condition, and the maximum displacement of the oscillation does not exceed 0.13 mm.

V. EFFECT OF VARIATION OF FESS PARAMETERS ON ROTOR DISPLACEMENT

Due to the use of axial passive magnetic bearings, it is not possible to form a closed-loop control through the control current. The combined force on the rotor consists of two parts: the electromagnetic force of the motor and the bearing capacity, when the combined force and gravity are not equal, rotor displacement will occur. In order to minimize the rotor displacement, it can only be achieved by increasing the air gap or bearing capacity, so that the influence of the electromagnetic force on the rotor is reduced. Therefore, it is necessary to study the influence of the main parameters, so as to ensure

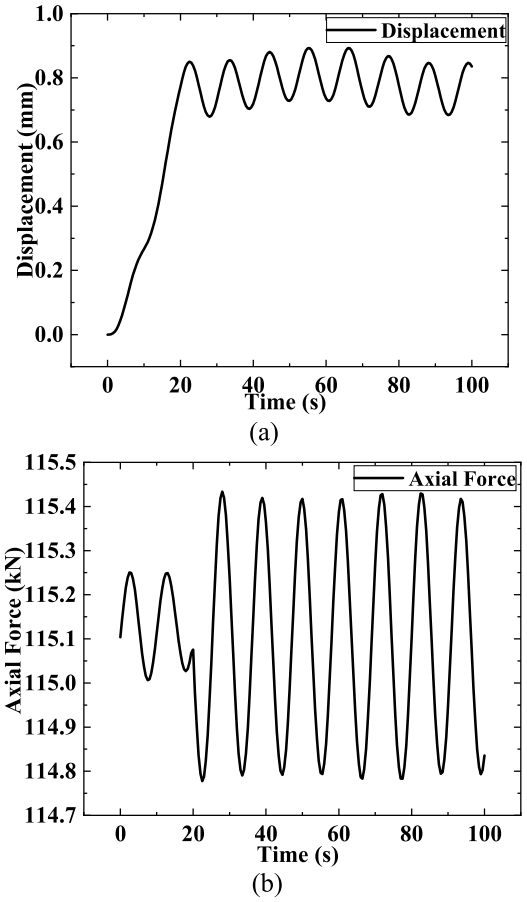

FIGURE 12. Results for motor air gap of 10 mm. (a) Displacement of the rotor. (b) Axial force of the rotor.

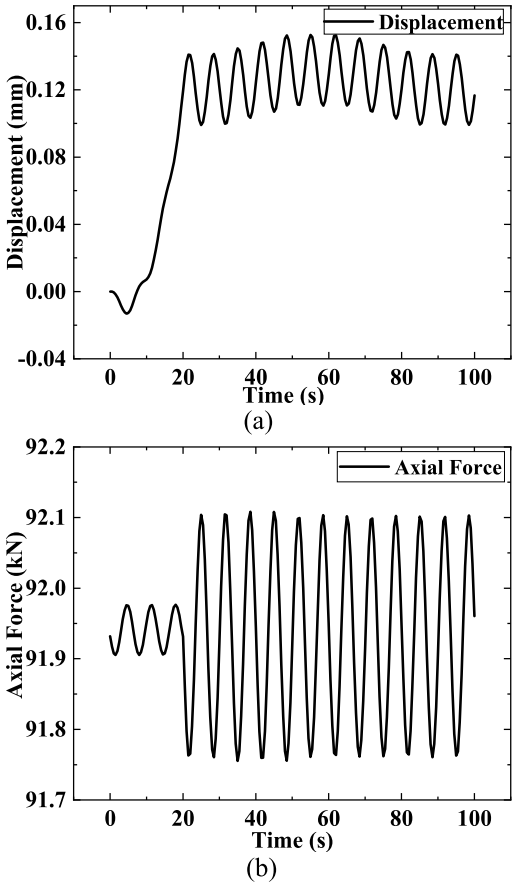

FIGURE 13. Results for motor air gap of 2 mm. (a) Displacement of the rotor. (b) Axial force of the rotor.

that the small vibration of the rotor within the controllable range.

According to Table 2 and the above research results, firstly, take the motor as an example. When the motor air gap is 6 mm, rotor weight is 10000 kg, and the PMB air gap is 6mm, the motor electromagnetic force is about 23 kN and the bearing carrying capacity is about 77 kN, and the electromagnetic force is about 30% of the bearing carrying capacity, which accounts for 23% of the total combined force of the rotor, so the maximum displacement obtained by the MATLAB calculation is about 0.285 mm. similarly for the generator, when the generator air gap is 6 mm, rotor weight is 10000 kg, and PMB air gap is 6 mm, the generator electromagnetic force is about 22.5 kN, bearing carrying capacity is about 77.36 kN, electromagnetic force is about 29% of bearing carrying capacity, accounting for 22.5% of the total combined force of the rotor, and the maximum displacement calculated by MATLAB is about 0.62 mm.

A. EFFECT OF AIR GAP VARIATION ON ROTOR DISPLACEMENT

1) MOTOR CONDITION

When the motor air gap increases, the motor electromagnetic force decreases. When the motor air gap is 10 mm and other parameters are constant, F_1 and F_2 under different currents and displacements are obtained by simulation.The RSM function of displacement, current and F_1 is obtained by fitting the relationships as in (16).The relationship between displacement and F_2 is unchanged.

$$F_1 = -0.001903 + 1.442x - 0.001163i + 0.1139x^2 + 0.0003328xi + 4.887\text{E} - 06i^2 \quad (16)$$

Further the differential equation of rotor motion is obtained as in (17) below and its initial value as in (18).

$$\dot{x} = -0.8317x - 0.0001163i + 0.01139x^2 + 0.00003328xi + 4.88\text{E} - 07i^2 \quad (17)$$

$$\begin{cases} x(1) = 0 \\ z(1) = 0 \\ y(1) = 0 \end{cases} \quad (18)$$

Similarly the above differential equations are solved separately using ode45 to find the displacement and force of the rotor as shown in Fig. 12. As the input current increases, the rotor vibrates axially and the maximum displacement is about 0.146 mm, which is less than the case of air gap of 6 mm. Therefore as the air gap increases, the electromagnetic force of the motor is smaller, accounting for 15.85% of the total

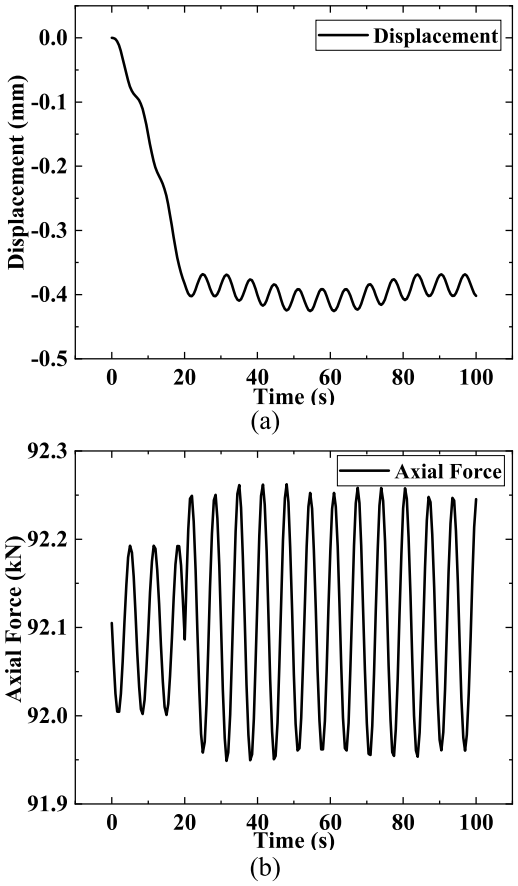

FIGURE 14. Results for generator air gap of 10 mm. (a) Displacement of the rotor. (b) Axial force of the rotor.

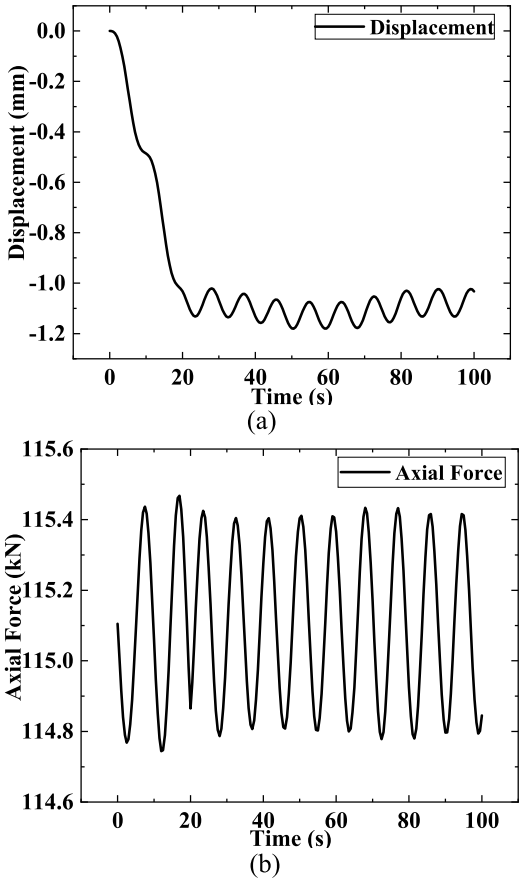

FIGURE 15. Results for generator air gap of 2 mm. (a) Displacement of the rotor. (b) Axial force of the rotor.

force of the rotor, and the effect caused by the current change on the rotor displacement is reduced.

Similarly when the motor air gap decreases, the electromagnetic force increases. When the motor air gap is 2 mm and the rest of the parameters are unchanged, the RSM function of displacement, current and F_1 is obtained by fitting the above relationship as in (19), and the relationship between displacement and F_2 remains unchanged.

$$F_1 = -0.006467 + 5.029x + 0.002803i + 0.3843x^2 + 0.0005438xi + 4.598\text{E} - 06i^2 \quad (19)$$

The differential equation of rotor motion is further obtained as in (20) with constant initial values.

$$\dot{x} = -0.473x + 0.0002803i + 0.03843x^2 + 0.0005438xi + 4.598\text{E} - 07i^2 \quad (20)$$

Again using ode45 to solve the above differential equations separately, the displacement and force of the rotor are obtained as shown in Fig. 13. As the input current increases, axial vibration occurs in the rotor and the maximum displacement is about 0.745 mm, which is greater than the condition where the air gap is 6 mm. Thus as the air gap decreases, the electromagnetic force on the rotor is larger, accounting for 32.78% of the total combined force on the rotor, and the effect caused by the current change on the rotor displacement becomes larger.

2) GENERATOR CONDITION

Similarly, for generator, when the air gap is increased to 10 mm and other parameters are kept constant, the RSM functions of displacement, current and F_1 are obtained by fitting the relationship as shown in (21). Further differential equations are shown in (22).

$$F_1 = -0.1682 + 1.663x - 0.01043i + 0.1072x^2 - 0.0009602xi + 5.745\text{E} - 06i^2 \quad (21)$$

$$\dot{x} = -0.8256x - 0.0001955i + 0.01081x^2 - 0.00002302xi - 9.504\text{E} - 06i^2 \quad (22)$$

The above differential equations are solved separately using ode45 to find the displacement and force of the rotor as shown in Fig. 14. As the air gap increases, the electromagnetic force of the generator is smaller, accounting for 16% of the total force of the rotor. Thus the effect of current variation on rotor displacement decreases and the maximum displacement is reduced to 0.426 mm when the air gap is 10 mm.

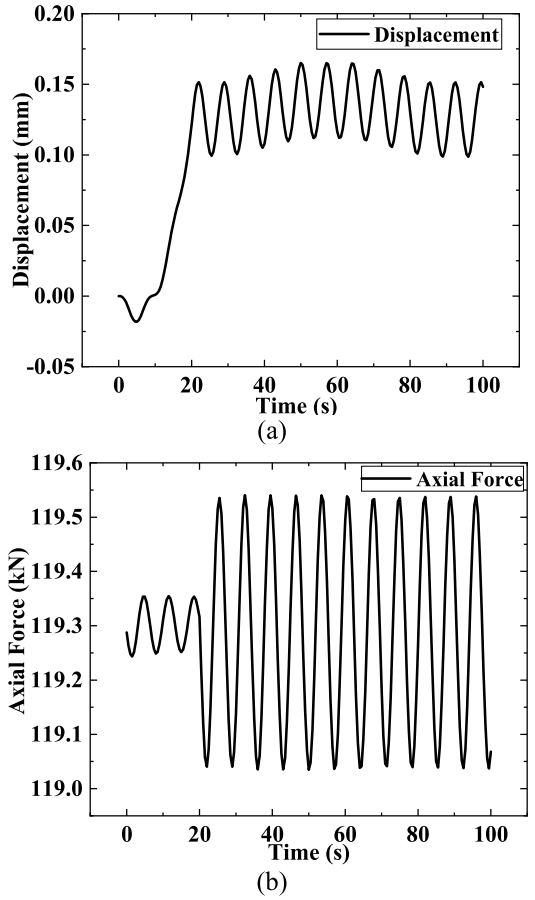

FIGURE 16. Results of motor condition with bearing capacity increasing. (a) Displacement of the rotor. (b) Axial force of the rotor.

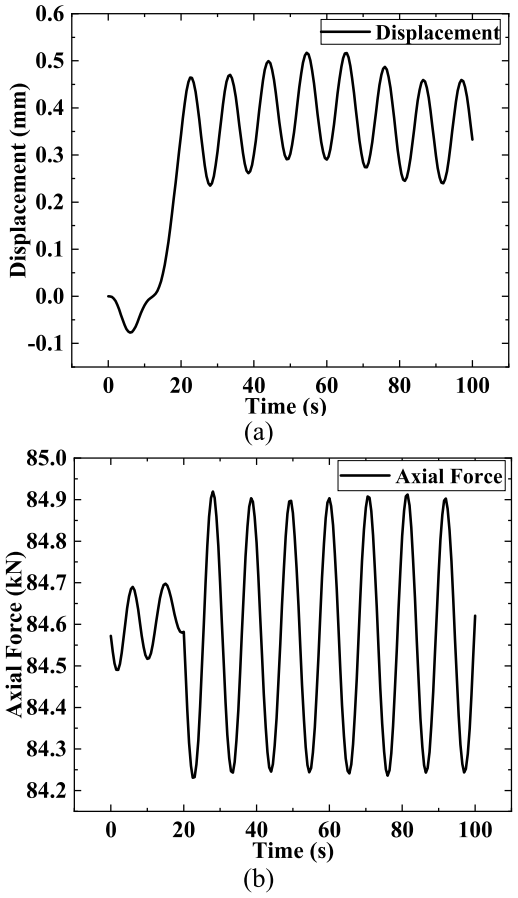

FIGURE 17. Results of motor condition with bearing load capacity decreasing. (a) Displacement of the rotor. (b) Axial force of the rotor.

When the generator air gap is 2 mm and the other parameters are unchanged, the RSM function of displacement, current and F_1 is obtained by fitting the relationship as in (23), and the relationship between displacement and F_2 remains constant. Further the differential equation is obtained as in (24).

$$F_1 = -0.004966 + 5.278x - 0.008229i + 0.3688x^2 - 0.0009076xi - 7.577\text{E}-06i^2 \quad (23)$$

$$\dot{x} = -0.4481x - 0.0008229i + 0.03688x^2 - 0.00009076xi + 7.577\text{E}-06i^2 \quad (24)$$

Again using ode45 to solve the above differential equations separately, the displacement and force of the rotor are obtained as shown in Fig. 15. As the input current increases, axial vibration occurs in the rotor and the maximum displacement is about 1.18 mm, which is greater than the condition where the air gap is 6mm. Thus as the air gap decreases, the electromagnetic force on the rotor is larger, accounting for 32.78% of the total combined force on the rotor, and the effect caused by the current change on the rotor displacement becomes larger.

B. EFFECT OF BEARING CAPACITY ON ROTOR DISPLACEMENT

1) MOTOR CONDITION

Firstly, for the motor condition, the electromagnetic force is kept constant, and when the bearing capacity is increased to 1.25 times of the original capacity, the relationship between the force and displacement can be fitted as (25), and the corresponding differential equation of motion is as follows (26), with constant initial value. The above differential equations are solved separately using the RK4 method, and the displacement and force of the rotor are obtained as shown in Fig. 16. As the input current increases, axial vibration occurs in the rotor and the maximum displacement decreases from 0.285 mm to 0.165 mm. With the increase in bearing capacity, the electromagnetic force remains unchanged, but its percentage of the total force on the rotor decreases to 18.9%, and the effect caused by the current change on the rotor displacement decreases.

$$F_2 = 96.7 - 12.2x \quad (25)$$

$$\dot{x} = -0.9648x - 0.0002765i + 0.01903x^2 + 0.0003705xi + 7.938\text{E}-07i^2 \quad (26)$$

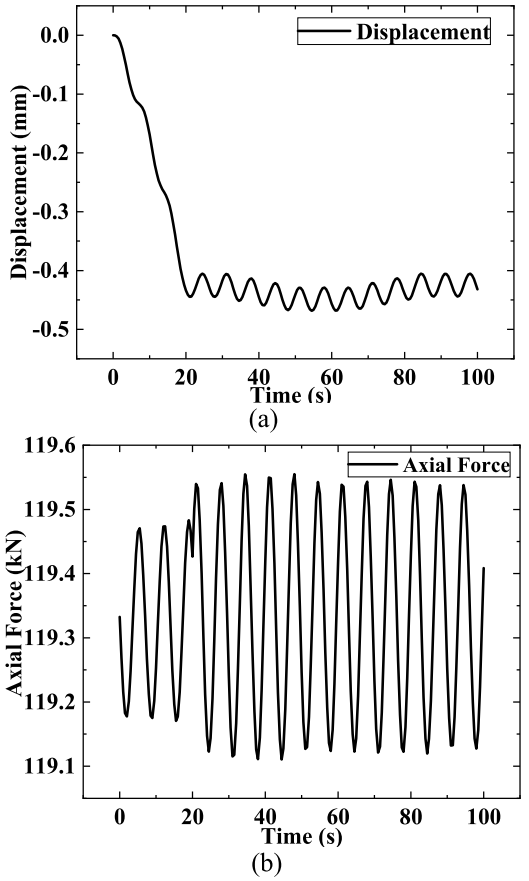

FIGURE 18. Results of generator condition with bearing capacity increasing. (a) Displacement of the rotor. (b) Axial force of the rotor.

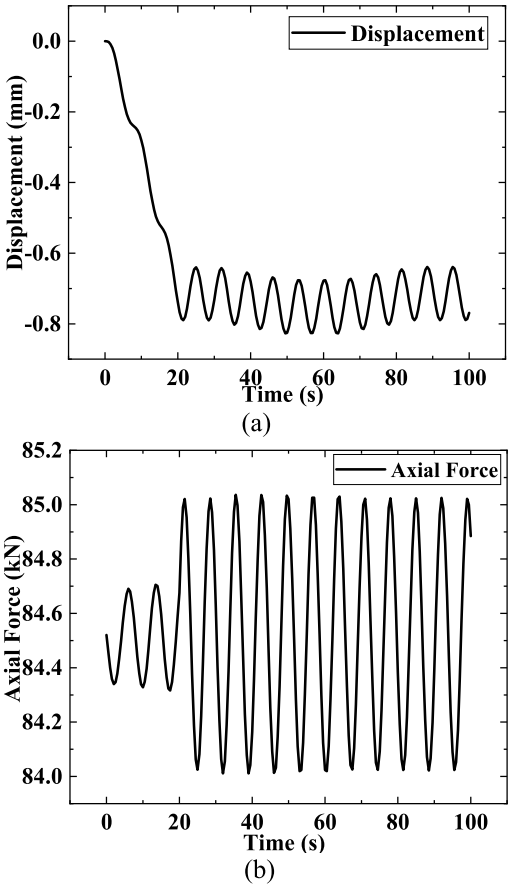

FIGURE 19. Results of generator condition with bearing load capacity decreasing. (a) Displacement of the rotor. (b) Axial force of the rotor.

Similarly when the bearing bearing capacity is reduced to 0.8 times of the original, the relationship between the force and displacement can be fitted to (27), and the corresponding differential equations of motion are as follows (28). The above differential equations are solved separately using ode45 to find the displacement and force of the rotor as shown in Fig. 17. As the input current increases, the rotor is displaced and vibrates, and the maximum displacement increases from 0.285 mm to 0.517 mm. Although the bearing capacity decreases and the electromagnetic force remains unchanged, its percentage of the total force on the rotor increases to 26.8%, so that the effect of current change on the displacement of the rotor is larger.

$$F_2 = 61.888 - 7.8072x \tag{27}$$

$$\dot{x} = -0.5255x - 0.0002765i + 0.01903x^2 + 0.0003705xi + 7.938\text{E} - 07i^2 \tag{28}$$

2) GENERATOR CONDITION

Similarly for the generator, when the bearing capacity is increased to 1.25 times of the original, the displacement and force of the rotor are obtained as shown in Fig. 18. As the bearing carrying capacity increases, the electromagnetic force on the rotor remains constant, which accounts for 18.9% of the total force, and the maximum rotor displacement for the change in current decreases from 0.623 mm to 0.48 mm.

Similarly, when the bearing capacity is reduced to 0.8 times of the original, the rotor displacement and force of the generator are obtained as shown in Fig. 19. Although the bearing capacity is reduced, the electromagnetic force remains unchanged and its percentage of the total rotor force increases to 36.65%, which in turn increases the maximum axial displacement from 0.623 mm to 0.826 mm.

C. EFFECT OF THE RATIO OF ELECTROMAGNETIC AND BEARING CAPACITY ON ROTOR DISPLACEMENT

From the above analysis, it is seen that the overall effect of current variation on the electromagnetic force of the machine is small, and the displacement decreases when the motor air gap increases or the bearing capacity increases. Therefore, when designing the machine, it is necessary to consider the effects of the PMB capacity and the unilateral electromagnetic force of the AFPMSM on axial vibration. While ensuring that the machine performance requirements are satisfied, the axial vibration displacement can be minimized by increasing machine air gap and bearing capacity. According to the structure of axial PMB, it can be seen that the bearing

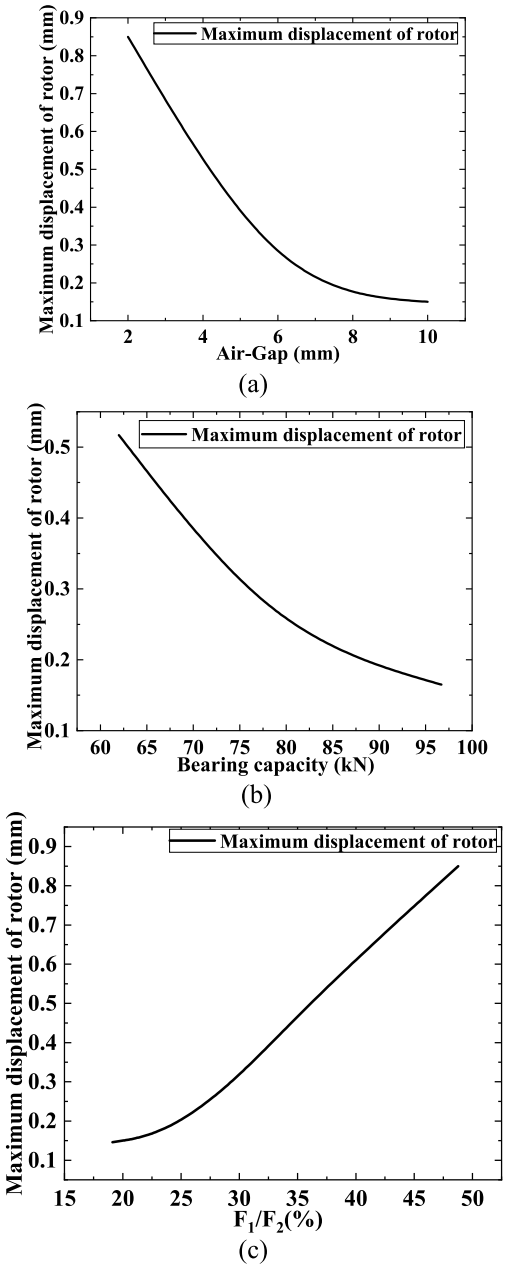

FIGURE 20. Variation of parameters with maximum displacement for motor. (a) Air gap. (b) Bearing capacity. (c) Ratio of electromagnetic force to bearing capacity.

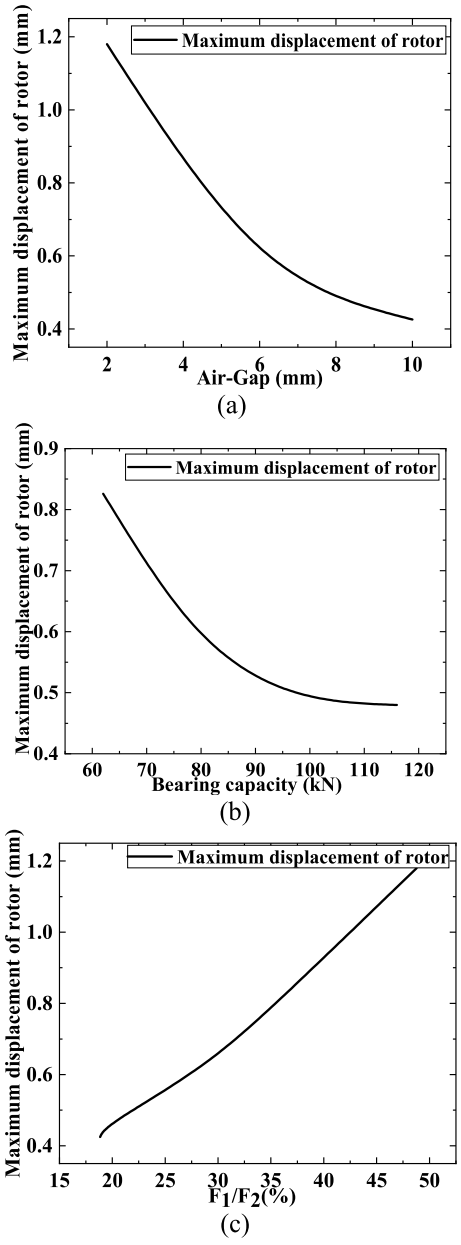

FIGURE 21. Variation of parameters with maximum displacement for generator. (a) Air gap. (b) Bearing capacity. (c) Ratio of electromagnetic force to bearing capacity.

capacity is mainly related to the number of PM blocks, the radial thickness of PMs, and the axial height of PMs. From Fig. 7, it can be seen that increasing the number of PM blocks, radial thickness of PMs and axial height of PMs can increase the bearing capacity and thus reduce the axial displacement.

To ensure reliable operation of the FESS, the rotor displacement should be less than the size of the air gap. When the structural parameters of the bearing is unchanged, from the above analysis, the relationship between the variation of motor parameters and the maximum rotor displacement under motor and generator conditions is fitted as shown in Fig. 20 and 21.

From the figure, it can be seen that the maximum rotor displacement decreases with the increase of air gap and bearing capacity. In turn, the relationship between the ratio of electromagnetic force and bearing capacity and the maximum rotor displacement is obtained. For the motor condition, when the ratio of electromagnetic force and bearing force is less than 35%, the maximum rotor displacement does not exceed 0.5 mm.

For generator condition, the load variation has an effect on the generator, but the effect is greater than for the motor condition. As can be seen from the figure, the ratio of electromagnetic force to bearing force needs to be less than 40% if the maximum rotor displacement is not to exceed 1 mm.

FIGURE 22. FESS prototype.

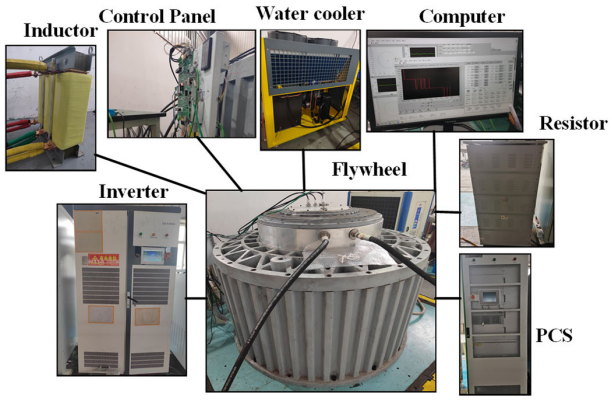

FIGURE 23. FESS experimental platform.

In conclusion, the ratio of electromagnetic force to bearing force can be increased by reasonably designing the bearing parameters and increasing the machine air gap, which makes it possible to minimize the axial vibration displacement of the flywheel rotor.

VI. PROTOTYPE EXPERIMENT

Based on the above theoretical and simulation analyses, a 450MJ/500kW FESS prototype based on a AFPMSM is designed and fabricated as shown in Fig. 22, and the FESS experimental platform as shown in Fig. 23. The required experimental equipment mainly includes 450 MJ/500 kW FESS, inverter, inductor, resistor box, water cooler, power control system (PCS), control panel, computer, oscilloscope, displacement sensors and so on.

Afterwards, C&D experiment is carried out on the flywheel, and due to the current limitation of the inductor, the peak current of 750 A is given to make the flywheel accelerated charging and decelerated discharging in the operating speed interval from 0 rpm to the rated speed of 5400 rpm. And after that, the one-phase C&D currents of the FESS at the rated speed are measured by oscilloscope as shown in Fig. 24. From the figure, it can be seen that the current waveforms are basically sinusoidal, in which the RMS value of the charging phase current is 578.1 A, and the RMS value

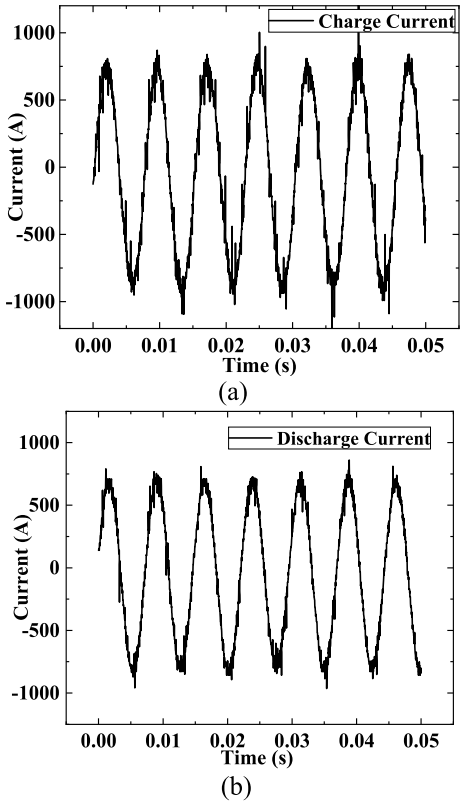

FIGURE 24. FESS one-phase C&D current waveforms.

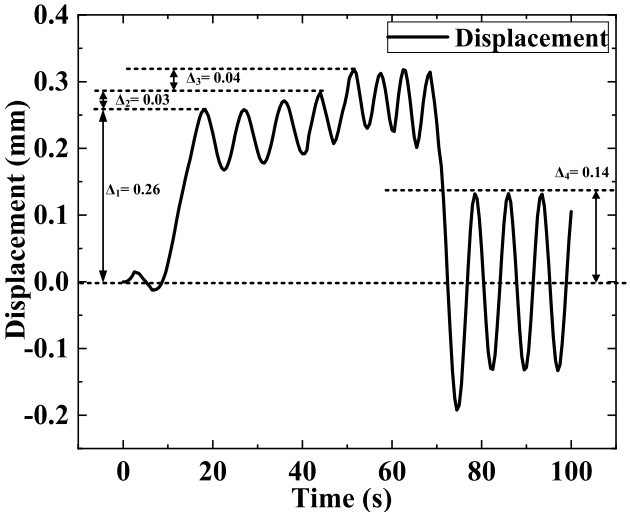

FIGURE 25. Experimental results of axial displacement of FESS.

of the discharging phase current is 480.7 A, which is basically close to the results of the FEM simulation with a small error.

Finally, experimental measurements of axial vibration displacements during charging, discharging and idling processes are carried out by installing axial displacement sensors on the flywheel rotor in order to accurately measure the axial displacement of the rotor. When the flywheel is started with rated current, it passes through charging, discharging and no-load processes successively, and the displacement corresponding

TABLE 3. Comparison of experimental results with FEM results.

Time/s	Current/ A	Axial Force/kN	FEM Displacement /mm	Experimental Displacement /mm
0-20	0-580	100.15	0.285	0.26
20-40	580-600	100.25	0.027	0.03
40-75	481-500	77.65	0.034	0.04
80-100	500-0	101	0.13	0.14

to the current change of each process is measured, as shown in Fig. 25. Firstly, the flywheel is charged and accelerated to start from the stopping state after 20 s, and the displacement of the starting process is 0.26 mm. After 10 s of charging and stabilizing operation, the current changed abruptly from the rated value of 580 A to 600 A, and the displacement increased by 0.03 mm. Then, the flywheel operated in the discharging process, with the displacement of the discharging current increasing from the rated value of 481 A to 500 A, and the displacement is 0.04 mm, which is slightly larger than the motor condition. Finally, after 20 s of discharging operation, the FESS is powered off and maintains no-load operation, and the maximum displacement at this time is about 0.14 mm. The time, displacement and current changes measured in the above experiments are compared with the FEM results in Table 3 below.Overall, this experimental result has a small error with the above analyzed results, and its maximum axial displacement is much smaller than the air gap, with stable operation of the FESS.

VII. CONCLUSION

In this paper, a AFPMSM and HALBACH axial PMB structure based on SMC material for high-capacity and high-power FESS is proposed in this paper, which has the advantages of short axial dimensions, high efficiency, low loss and compact structure. But the drawback of this structure is the presence of a large axial magnetic force between the stator and rotor, imposing high requirements on the axial bearing performance during machine operation. However, due to the uncontrollability of the PMB, the axial magnetic force of the AFPMSM will have a certain impact on the load carrying stability of the axial PMB, leading to axial vibrations during the operation of the flywheel. Therefore, the axial vibration of the 450 MJ/500 kW FESS based on AFPMSM is mainly researched in this paper. Firstly, a 3D FEM model of the machine and bearing are established, and the FEM is used to research the effects of current, air gap and bearing parameters on the rotor force. In addition, the relationship between the current and displacement on axial force is fitted by the RSM. The startup process and the effect of current change on displacement under three operating conditions of the FESS are investigated by the RK4 method. After that, the rotor displacements under different air gaps and bearing forces are investigated separately, and then the relationship between the ratio of electromagnetic force and bearing capacity and the maximum rotor displacement is deduced. Finally, a FESS prototype is fabricated and experimented, and the results are roughly the same as the analysis results. The above research is of great significance for the future development of high-capacity FESS based on AFPMSM and PMB, and the reliability of this novel flywheel structure is proved through the research. However, the current research only involves the influence of the dimensional parameters of the machine and bearing on the axial vibration through electromagnetic FEM simulation and numerical analysis. The optimization of axial vibration through advanced control strategies will be a direction for exploration in future research.

REFERENCES

[1] R. Arghandeh, M. Pipattanasomporn, and S. Rahman, "Flywheel energy storage systems for ride-through applications in a facility microgrid," *IEEE Trans. Smart Grid*, vol. 3, no. 4, pp. 1955–1962, Dec. 2012, doi: 10.1109/TSG.2012.2212468.

[2] G. Ren, G. Ma, and N. Cong, "Review of electrical energy storage system for vehicular applications," *Renew. Sustain. Energy Rev.*, vol. 41, pp. 225–236, Jan. 2015, doi: 10.1016/j.rser.2014.08.003.

[3] M. Farhadi and O. Mohammed, "Energy storage technologies for high-power applications," *IEEE Trans. Ind. Appl.*, vol. 52, no. 3, pp. 1953–1961, May 2016, doi: 10.1109/TIA.2015.2511096.

[4] H. Zhong, F. Teng, and M. A. Peñalba, "Editorial for the special issue on emerging technology and advanced application of energy storage in low-carbon power systems," *Chin. J. Electr. Eng.*, vol. 9, no. 3, pp. 1–2, Sep. 2023, doi: 10.23919/CJEE.2023.000035.

[5] R. Takarli, A. Amini, M. Khajueezadeh, M. S. Zarbil, A. Vahedi, A. Kiyoumarsi, H. Tarzamni, and J. Kyyra, "A comprehensive review on flywheel energy storage systems: Survey on electrical machines, power electronics converters, and control systems," *IEEE Access*, vol. 11, pp. 81224–81255, 2023, doi: 10.1109/ACCESS.2023.3301148.

[6] C. Ye, D. Yu, K. Liu, Y. Dai, C. Deng, J. Yang, and J. Zhang, "Research of a stator PM excitation solid rotor machine for flywheel energy storage system," *IEEE Trans. Ind. Electron.*, vol. 69, no. 12, pp. 12140–12151, Dec. 2022, doi: 10.1109/TIE.2021.3130323.

[7] Y. Chen, B. Zang, H. Wang, H. Liu, and H. Li, "Composite PM rotor design and alternating flux density harmonic component analysis of a 200 kW high-speed PMSM used in FESS," *IEEE Trans. Ind. Appl.*, vol. 59, no. 2, pp. 1469–1480, Mar. 2023, doi: 10.1109/TIA.2022.3218526.

[8] M. Sun, Y. Xu, and W. Zhang, "Multiphysics analysis of flywheel energy storage system based on cup winding permanent magnet synchronous machine," *IEEE Trans. Energy Convers.*, vol. 38, no. 4, pp. 2684–2694, Dec. 2023, doi: 10.1109/TEC.2023.3283504.

[9] W. Zhang, J. Wang, P. Zhu, and J. Yu, "A novel vehicle-mounted magnetic suspension flywheel battery with a virtual inertia spindle," *IEEE Trans. Ind. Electron.*, vol. 69, no. 6, pp. 5973–5983, Jun. 2022, doi: 10.1109/TIE.2021.3088375.

[10] K. Liu, M. Yin, W. Hua, Z. Ma, M. Lin, and Y. Kong, "Design and analysis of Halbach ironless flywheel BLDC motor/generators," *IEEE Trans. Magn.*, vol. 54, no. 11, pp. 1–5, Nov. 2018, doi: 10.1109/TMAG.2018.2833958.

[11] H. Wang, Z. Wu, K. Liu, J. Wei, and H. Hu, "Modeling and control strategies of a novel axial hybrid magnetic bearing for flywheel energy storage system," *IEEE/ASME Trans. Mechatronics*, vol. 27, no. 5, pp. 3819–3829, Oct. 2022, doi: 10.1109/TMECH.2022.3145705.

[12] Z. Wang, J. Yang, S. Dai, Y. Feng, and S. Huang, "Novel dual-rotor single-stator coreless permanent magnet machine with dual-flywheel," *IEEE Trans. Magn.*, vol. 58, no. 8, pp. 1–6, Aug. 2022, doi: 10.1109/TMAG.2022.3154749.

[13] Z. Kohari, "Test results of a compact superconducting flywheel energy storage with disk-type, permanent magnet motor/generator unit," *IEEE Trans. Appl. Supercond.*, vol. 19, no. 3, pp. 2095–2098, Jun. 2009, doi: 10.1109/TASC.2009.2018760.

[14] F. Marignetti, V. D. Colli, and S. Carbone, "Comparison of axial flux PM synchronous machines with different rotor back cores," *IEEE Trans. Magn.*, vol. 46, no. 2, pp. 598–601, Feb. 2010, doi: 10.1109/TMAG.2009.2034021.

[15] M. Sun, Y. Xu, and S. Chen, "Research on electromagnetic system of large capacity energy storage flywheel," *IEEE Trans. Magn.*, vol. 59, no. 5, pp. 1–5, May 2023, doi: 10.1109/TMAG.2023.3239981.
[16] Z. Zhang, C. Wang, and W. Geng, "Design and optimization of Halbach-array PM rotor for high-speed axial-flux permanent magnet machine with ironless stator," *IEEE Trans. Ind. Electron.*, vol. 67, no. 9, pp. 7269–7279, Sep. 2020, doi: 10.1109/TIE.2019.2944033.
[17] G. G. Sotelo, R. de Andrade Jr., and A. C. Ferreira, "Magnetic bearing sets for a flywheel system," *IEEE Trans. Appl. Supercond.*, vol. 17, no. 2, pp. 2150–2153, Jun. 2007, doi: 10.1109/TASC.2007.899268.
[18] H. Mitsuda, A. Inoue, B. Nakaya, and M. Komori, "Improvement of energy storage flywheel system with SMB and PMB and its performances," *IEEE Trans. Appl. Supercond.*, vol. 19, no. 3, pp. 2091–2094, Jun. 2009, doi: 10.1109/TASC.2009.2019533.
[19] S. Mukoyama, K. Nakao, H. Sakamoto, T. Matsuoka, K. Nagashima, M. Ogata, T. Yamashita, Y. Miyazaki, K. Miyazaki, T. Maeda, and H. Shimizu, "Development of superconducting magnetic bearing for 300 kW flywheel energy storage system," *IEEE Trans. Appl. Supercond.*, vol. 27, no. 4, pp. 1–4, Jun. 2017.
[20] L. Xu, Y. Xu, and J. Gong, "Analysis and optimization of cogging torque in yokeless and segmented armature axial-flux permanent-magnet machine with soft magnetic composite core," *IEEE Trans. Magn.*, vol. 54, no. 11, pp. 1–5, Nov. 2018, doi: 10.1109/TMAG.2018.2850317.
[21] Y. Le, J. Fang, and J. Sun, "Design of a Halbach array permanent magnet damping system for high speed compressor with large thrust load," *IEEE Trans. Magn.*, vol. 51, no. 1, pp. 1–9, Jan. 2015, doi: 10.1109/TMAG.2014.2335715.
[22] W.-H. Kim, C.-W. Kim, H.-S. Shin, S.-S. Jeong, and J.-Y. Choi, "Optimal design of short-stroke linear oscillating actuator for minimization of side force using response surface methodology," *IEEE Trans. Magn.*, vol. 58, no. 2, pp. 1–5, Feb. 2022, doi: 10.1109/TMAG.2021.3088453.
[23] H. L. Li, S. L. Ho, and W. N. Fu, "Application of multi-stage diagonally-implicit Runge–Kutta algorithm to transient magnetic field computation using finite element method," *IEEE Trans. Magn.*, vol. 48, no. 2, pp. 279–282, Feb. 2012, doi: 10.1109/TMAG.2011.2175481.
[24] S.-M. Lee, S.-H. Lee, H.-S. Choi, and I.-H. Park, "Reduced modeling of eddy current-driven electromechanical system using conductor segmentation and circuit parameters extracted by FEA," *IEEE Trans. Magn.*, vol. 41, no. 5, pp. 1448–1451, May 2005, doi: 10.1109/TMAG.2005.844549.

MINGXIN SUN was born in Shandong, China. She received the B.Sc. degree in electrical engineering from the China University of Mining and Technology, Xuzhou, China, in 2019. She is currently pursuing the Ph.D. degree in electrical engineering with the School of Electrical Engineering, Shandong University, Jinan, China. Her research interests include the key technology research of large-capacity and high-power energy storage flywheel.

YANLIANG XU was born in Shandong, China. He received the B.S. and M.Sc. degrees in electrical machines from the Shandong University of Technology, Shandong, in 1989 and 1994, respectively, and the Ph.D. degree in electrical machines from the Shenyang University of Technology, Shenyang, China, in 2001. He is currently a Professor with the School of Electrical Engineering, Shandong University. He is the Head of the Institute of Electrical Machines. His research interest includes electrical machines.